Nanoscale

PAPER

View Article Online
View Journal | View Issue

Cite this: *Nanoscale*, 2025, **17**, 22260

Hole scavenger concentration dependent photoreduction pathway of nitrobenzene catalyzed by CdS quantum dots

Chao Wang,[a] Hawi N. Nyiera,[a] Charlotte Fuqua,[a] Courtney Brea,[b] Guoxiang Hu,[c,d] Tomoyasu Mani[a] and Jing Zhao *[a]

Hole scavengers are often employed in photocatalytic reactions catalyzed by semiconductors to efficiently extract photogenerated holes, thereby suppressing charge recombination and enhancing the overall catalytic activity. Beyond improving charge separation, the type of hole scavengers can also affect the activity, selectivity, and mechanism of the reaction. Interestingly, our findings in this work reveal that not only the identity but also the amount of hole scavenger plays a significant role, indicating the reaction pathway. Specifically, in nitrobenzene reduction catalyzed by CdS quantum dots (QDs), the concentration of hole scavenger Na_2SO_3 influences the reaction pathway and the final products: low concentrations (2–8 mM) favored the direct reduction pathway and yielded phenylhydroxylamine and aniline, while high concentrations (12–24 mM) favored an indirect (coupling) pathway and produced azoxybenzene. We hypothesized that $SO_4^{\bullet-}$ radicals formed at high concentrations of Na_2SO_3 in the presence of dissolved oxygen is responsible for this change in reduction pathway. The existence of $SO_4^{\bullet-}$ radicals was validated by Electron Spin Resonance spectroscopy. Quenching of $SO_4^{\bullet-}$ radicals using *tert*-butyl alcohol (TBA) reverted the reaction back to the direct reduction pathway even when a high concentration of Na_2SO_3 was added, confirming the critical role of $SO_4^{\bullet-}$. Density functional theory calculations revealed that the $SO_4^{\bullet-}$ adsorbed onto the CdS surface abstracts hydrogen from the reaction intermediates, promoting the indirect coupling reaction. In addition, photoluminescence and femtosecond transient absorption studies showed that rapid hole trapping in CdS QDs occurred within 3–4 picoseconds after excitation, and Na_2SO_3 scavenged trapped holes at a timescale of tens of nanoseconds. These findings highlight the diverse functions of hole scavengers in photocatalysis. Their quantity and the species generated after hole scavenging can direct the reaction pathways and product selectivity.

Received 21st July 2025,
Accepted 11th September 2025

DOI: 10.1039/d5nr03085d

rsc.li/nanoscale

Introduction

Colloidal quantum dots (QDs) are known to be efficient photocatalysts by absorbing light of proper energy and generating excited charge carriers that drive a range of chemical reactions, such as water splitting,[1–4] CO_2 reduction,[5–10] and decomposition of environmental pollutants.[11,12] In photo reduction reactions catalyzed by QDs or QD-based hybrid structures, photoexcited electrons in QDs are transferred from their conduction band to the reactants or other components in the hybrid structures, leaving holes in the valence band.[13] To reduce the recombination of the photoexcited electrons with holes and prevent QDs from photooxidation, hole scavengers are usually added to the reaction systems. Hole scavenger molecules donate electrons to the holes, thereby making the photoexcited electrons more available for reaction and improving the overall catalytic efficiency and stability of the system.[14,15]

The chemical nature of the scavengers is a factor that affects the photocatalytic activity of QDs-catalyzed reactions.[16] For example, Jin *et al.* reported that adding ascorbic acid to hybrid CdS/ZnS QD-Au nanoparticles led to significantly higher H_2 evolution rate compared to using methanol, Na_2S&Na_2SO_3, or triethanolamine as a hole scavenger. The improvement in H_2 evolution was ascribed to the acidic environment provided by ascorbic acid.[17] Li *et al.* reported that the addition of an H_2S-saturated Na_2S&Na_2SO_3 solution to

[a]*Department of Chemistry, University of Connecticut, Storrs, Connecticut 06269-3060, USA. E-mail: jing.zhao@uconn.edu*
[b]*Department of Chemistry and Biochemistry, Queens College of the City University of New York, New York, NY 11367, USA*
[c]*School of Materials Science and Engineering, Georgia Institute of Technology, Atlanta, GA 30332, USA*
[d]*School of Chemistry and Biochemistry, Georgia Institute of Technology, Atlanta, GA 30332, USA*

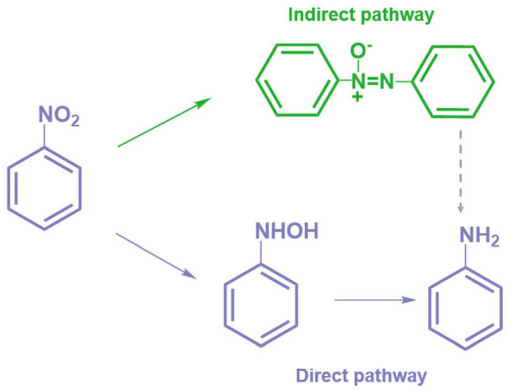

Scheme 1 Illustration of the reduction reaction of nitrobenzene.

hybrid CdS/PdS nanoparticles yielded a maximum H_2 production rate approximately 13.7 times higher than that achieved using triethanolamine, sodium ascorbate, methanol, or formic acid as hole scavengers, due to its higher ability in removing the holes accumulated on the surface of the catalysts.[18] Hole scavengers have also been found to improve interfacial charge transfer in hybrid nanocrystal/molecular catalysts, potentially favoring photocatalytic reduction reactions.[19] These reports show that the roles of hole scavengers are very complex and vary in different reaction systems.

In our recent work, we observed that in the photo-reduction of nitrobenzene catalyzed by CdS QDs, the type of hole scavengers used not only significantly influenced reaction rates, but also affected the reaction pathways and final products. When methanol, 3-mercaptopropionic acid, ascorbic acid, or ammonium formate were employed as the hole scavenger, nitrobenzene followed a "direct" reaction pathway, producing phenylhydroxylamine and aniline. However, when sodium sulfite (Na_2SO_3) was used as a hole scavenger, nitrobenzene followed the "indirect" or "coupling" reaction pathway, producing azoxybenzene.[20] The reaction pathway is illustrated in Scheme 1.[21–24] To explain why Na_2SO_3 changes the selectivity of the reaction, we performed systematic studies using different concentrations (2–24 mM) of Na_2SO_3 in this work. Surprisingly, we observed that at low concentrations of Na_2SO_3 (2–8 mM), the reaction followed the direct reduction pathway; while at high Na_2SO_3 concentrations (12–24 mM), coupling product azoxybenzene was obtained. We showed that after scavenging the holes on CdS, SO_3^{2-} turned into $SO_4^{\bullet-}$ radicals under certain conditions, and the $SO_4^{\bullet-}$ on the CdS surface promoted the indirect reaction pathway and led to different reaction products.

Results and discussion

The absorption spectra of CdS QDs in water after ligand exchange with MPA exhibit features similar to previously reported spectra of CdS QDs with the first excitonic peak at 455 nm (Fig. S1a).[20] Furthermore, the CdS QDs were mixed with 2, 4, 8, 12, 16, and 24 mM Na_2SO_3. The absorption spectra of the mixtures are almost identical to that of the QDs alone, suggesting that the addition of Na_2SO_3 does not alter the electronic structure or bandgap of the CdS QDs. The transmission electron microscopy (TEM) image (Fig. S1b) reveals that the QDs have an average size of approximately 6 nm, which aligns with the size calculated from the first excitonic peak.[25] The CdS QDs were transferred into water and used for the photocatalytic reaction of nitrobenzene following a published procedure.[20] Briefly, 0.35 μM CdS QDs was mixed with 2.5 mM nitrobenzene and varying amounts of Na_2SO_3 from 2–24 mM in D_2O : CD_3OD (v : v%) = 4 : 1 solvent, buffered to 9–11 pH with 0.2 M tri buffer. The estimated molar ratio of CdS : Na_2SO_3 ranges from $1 : 5.7 \times 10^3$ to $1 : 6.9 \times 10^4$. The reaction solution was purged with house N_2 gas unless otherwise noted. House N_2 gas was produced from 99.999% pure liquid N_2 but may become contaminated with air during distribution through the piping system. The cuvette was then excited with a 450–460 nm LED with a photon flux of 2.2×10^{17} photons per s per cm^2 for the desired reaction time and the product was analyzed by ^{1}H-NMR without further purification. The reference NMR spectra of nitrobenzene, nitrobenzene with CdS QDs, phenylhydroxylamine, azoxybenzene, and aniline are shown in Fig. S2. As shown in the NMR spectra of the reaction product when 16 mM Na_2SO_3 was added (Fig. 1a), the azoxybenzene (Ph–N═N(O)–Ph) peaks appeared at 7.14–7.66 ppm between 2 and 6 hours of reaction. This suggests that the reduction of nitrobenzene (Ph–NO_2) catalyzed by CdS QDs follows the "indirect" reaction pathway under this condition, consistent with our previous report. Further increasing the Na_2SO_3 concentration to 24 mM led to stronger azoxybenzene peaks persisting throughout the 6-hour reaction (Fig. S3d). Interestingly, when a low concentration of 2 mM Na_2SO_3 was added (Fig. 1b), phenylhydroxylamine (PHA) peaks appeared at 6.85–6.93 and 7.14–7.25 ppm after 1 and 2 hours of reaction. After 4 and 6 hours of reaction, additional aniline (Ph-NH_2) peaks appeared at 6.64–6.72 ppm and 7.02–7.09 ppm. These are the products of the "direct" reduction pathway. Similar results were observed for 4 mM of Na_2SO_3 (Fig. S3a) except that aniline peaks began to appear at 2 h and became more pronounced at 4 and 6 h. When 8 mM Na_2SO_3 was added (Fig. S3b), phenylhydroxylamine peaks appeared at 2 and 4 hours, and aniline peaks appeared at 6 hours. However, when Na_2SO_3 concentration was further increased to 12 mM, product from the indirect pathway, azoxybenzene, was observed at 6 hours (Fig. S3c). Thus, we conclude that the nitrobenzene reduction pathway is dependent on the hole scavenger Na_2SO_3 concentration, with the transition range falling between 8 mM and 12 mM. Below this transition range, the production of aniline is faster when increasing Na_2SO_3 concentration from 2 to 4 mM. Within the transition range, slower formation of aniline is observed at 8 mM Na_2SO_3 and the product switched to azoxybenzene at 12 mM Na_2SO_3. Above the transition concentration, a higher rate of azoxybenzene formation is observed when Na_2SO_3 concentration increases to 16 mM and 24 mM. These results show that the amount of hole scavengers can affect the reaction pathways and rates of photocatalytic reactions.

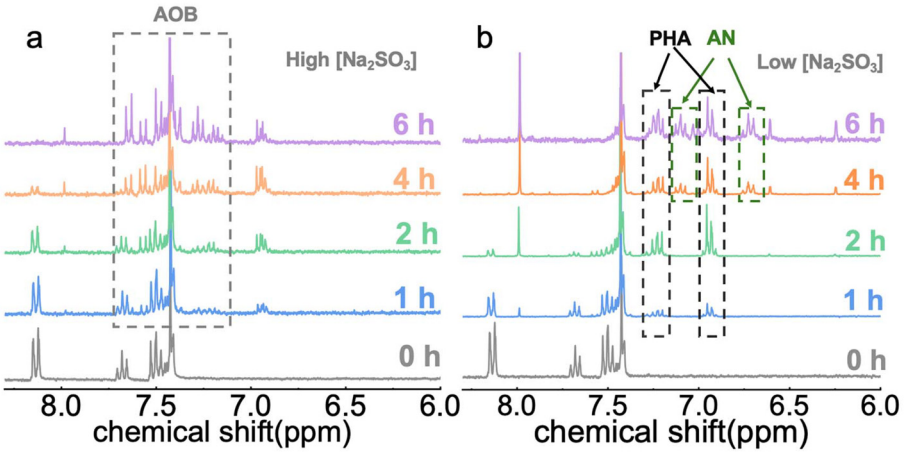

Fig. 1 ^{1}H-NMR results of the products during photocatalysis of nitrobenzene using CdS QDs at 0 h, 1 h, 2 h, 4 h, and 6 h with (a) high (16 mM) concentration Na_2SO_3, (b) low (2 mM) concentration Na_2SO_3. The reaction solutions were purged with house N_2. AOB: azoxybenzene; PHA: phenylhydroxylamine; AN: aniline.

Based on the photocatalytic results, we hypothesize that sulfite ions (SO_3^{2-}) and their product after donating electrons to the catalysts may be involved in the reaction. As hole scavengers, SO_3^{2-} can be oxidized by the photogenerated holes in CdS QDs to form sulfite radicals ($SO_3^{\bullet-}$) *via* a hole-mediated oxidation process (eqn (1)), as illustrated in Fig. 2a. $SO_3^{\bullet-}$ radicals can then react with dissolved oxygen to form $SO_5^{\bullet-}$ radicals (eqn (2)); subsequently, $SO_5^{\bullet-}$ can be reduced by excess SO_3^{2-} to form $SO_4^{\bullet-}$ radicals (eqn (3)).[26,27]

$$SO_3^{2-} + h^+ \rightarrow SO_3^{\bullet-}, \quad k = 1.9 \times 10^9\ M^{-1}\ s^{-1} \qquad (1)$$

$$SO_3^{\bullet-} + O_2 \rightarrow SO_5^{\bullet-}, \quad k = 1.3 \times 10^7\ M^{-1}\ s^{-1} \qquad (2)$$

$$SO_5^{\bullet-} + SO_3^{2-} \rightarrow SO_4^{\bullet-} + SO_4^{2-}, \quad k = 2.0 \times 10^9\ M^{-1}\ s^{-1} \qquad (3)$$

The rate constants (k) in eqn (1)–(3) are taken from Ranguelova *et al.*[28] $SO_4^{\bullet-}$ radicals are known to abstract –H from a variety of organic molecules.[29,30] Presumably, its participation in the nitrobenzene reduction reaction could affect the reduction pathway. Note that hydroxyl radicals have also been reported to affect the reaction pathway[31] and we do not rule out their participation in this reaction. Our observations clearly showed the importance of sulfur-containing species, and thus we focus on those in this work. To examine whether $SO_4^{\bullet-}$ formed in the reaction solution, Electron Spin Resonance (ESR) measurements of sulfur-containing radicals were performed using 5,5-dimethyl-1-pyrroline-*N*-oxide (DMPO) as the spin-trap.[32] The samples were prepared by mixing DMPO, CdS QDs, and 2 mM or 16 mM Na_2SO_3 in air using water as the solvent, and were illuminated under 400 nm light during the ESR measurements. The sample with 2 mM Na_2SO_3 has a very weak signal that is hard to identify. In comparison, the one with 16 mM Na_2SO_3 exhibited a clear DMPO-$SO_4^{\bullet-}$ adduct signal (Fig. 2b, bottom two spectra, and the fitted spectra are shown in Fig. S4), proving the generation of $SO_4^{\bullet-}$ under this condition.[33] Since the formation of $SO_4^{\bullet-}$ requires O_2, we further tested if $SO_4^{\bullet-}$ can still be detected by ESR if O_2 is excluded.[27] To do that, N_2 from the gas cylinder (Airgas, >99.999% pure) was flowing through the solution before and during the ESR measurements. Both 2 mM and 16 mM Na_2SO_3-CdS QDs samples show a strong DMPO-$SO_3^{\bullet-}$ adduct signal[34] (Fig. 2b, top two spectra), confirming that the holes in photoexcited CdS QDs were scavenged by SO_3^{2-}, converting it to $SO_3^{\bullet-}$ (eqn (1)). Moreover, due to a lack of O_2, eqn (2) and (3) did not proceed, thus $SO_4^{\bullet-}$ was not detected. Note that an overall weaker ESR signal for the DMPO-$SO_4^{\bullet-}$ adduct, compared to those for the DMPO-$SO_3^{\bullet-}$, is likely due to its rapid conversion to the DMPO-OH adduct, not reflecting the concentrations of the radicals.[35]

The ESR results suggest that the purging gas affected $SO_4^{\bullet-}$ radical formation and therefore could have an impact on the nitrobenzene reduction pathway. Although all the reaction mixtures were purged with house N_2 for 5 minutes (details in SI section 1.3) prior to conducting the photocatalytic reactions presented in Fig. 1 and S3, we assume that there is still dissolved O_2 in the reaction solution due to the air in house N_2, leading to the formation of $SO_4^{\bullet-}$. To test this assumption, we investigated if different purging gases would alter the reaction pathway of nitrobenzene reduction at a high concentration of Na_2SO_3 above the transition range, *i.e.*, 16 mM, over a 4-hour reaction. The influence of protective gas on nitrobenzene reduction product has also been reported in previous studies.[36] We found that under purging with house N_2 or air, the reaction follows an "indirect" pathway, as evident by the appearance of azoxybenzene peaks in the NMR spectra in Fig. 2c. However, when the reaction solution was purged with N_2 or Ar from the gas cylinder, the reaction shifts to a "direct" pathway, resulting in the formation of phenylhydroxylamine and aniline. This study confirms that the dissolved O_2 influences the reaction pathway, likely due to the formation of $SO_4^{\bullet-}$.[27,37]

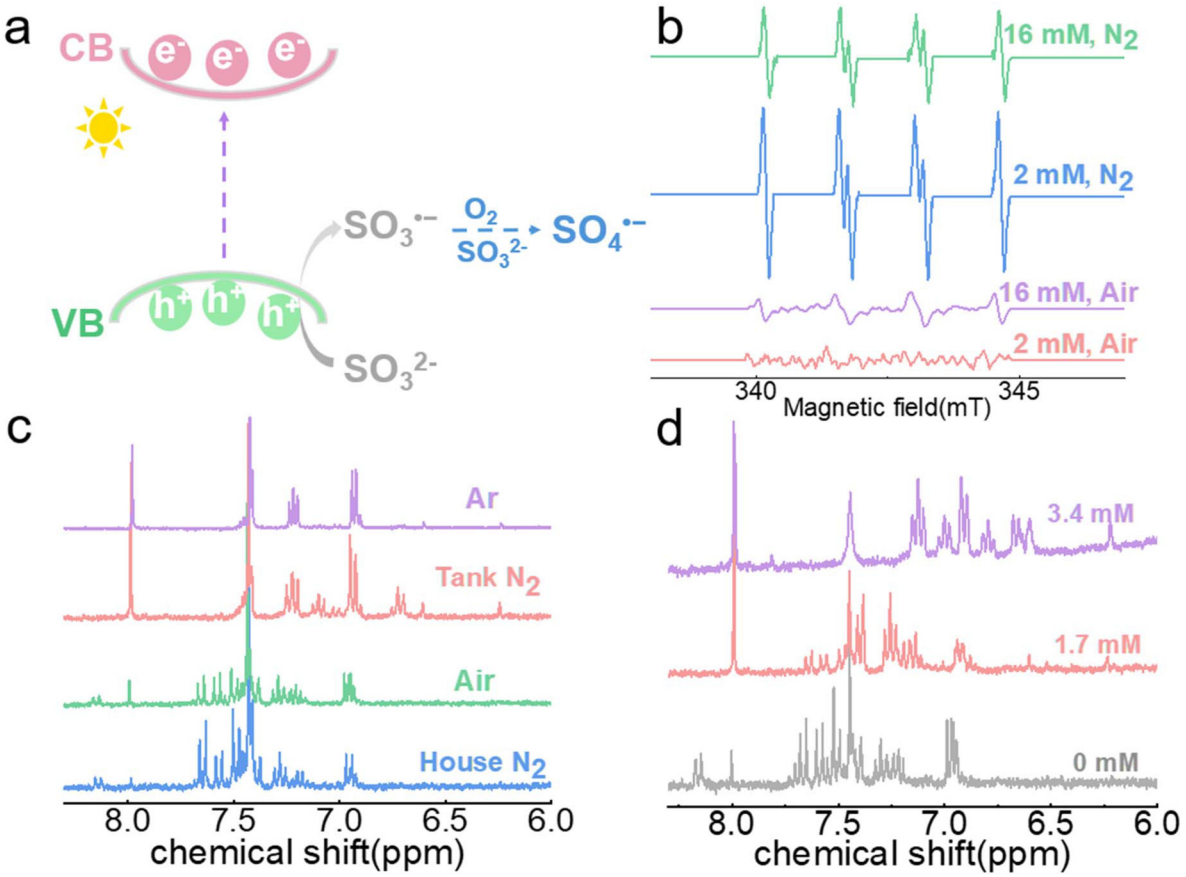

Fig. 2 (a) Schematic illustration of the potential transformation of SO_3^{2-}. (b) ESR spectra of DMPO (1.12 M), CdS QDs (0.35 μM), and Na_2SO_3 under 400 nm light taken in varying conditions: N_2 flow, 2 mM Na_2SO_3(blue); N_2 flow, 16 mM Na_2SO_3 (green); air, 2 mM Na_2SO_3 (pink); air, 16 mM Na_2SO_3 (purple). (c) NMR spectra of the products from nitrobenzene photocatalysis using CdS QDs and 16 mM Na_2SO_3 for 4 h. The reaction solution was purged with gases: house N_2(blue), air (green), tank N_2(pink), and tank argon(purple). (d) NMR spectra of the products from nitrobenzene photocatalysis using CdS QDs and 16 mM Na_2SO_3 for 4 h with different concentrations of *tert*-butanol purged with house N_2.

To further explore if $SO_4^{\bullet-}$ radicals are truly responsible for the reaction pathway, quenching experiments were carried out. Since the $SO_4^{\bullet-}$ radical is very sensitive to α-H, the rate constant (k) for its reaction with *tert*-butyl alcohol (TBA) with $SO_4^{\bullet-}$ is high ($k_{TBA,SO_4^{\bullet-}} = 4.0 - 9.1 \times 10^5\ M^{-1}\ s^{-1}$), making TBA an effective quencher for $SO_4^{\bullet-}$ radicals.[38] The quenching experiments were performed by adding increasing amounts of TBA (1.7 mM, and 3.4 mM) to the photocatalytic reaction mixture with 16 mM Na_2SO_3 over a 4-hour reaction period. As observed in Fig. 2d, the addition of TBA leads to different reaction products. Without TBA, the NMR spectrum resembles that of azoxybenzene, indicating the "indirect" pathway. At 1.7 mM TBA, the spectrum changed slightly with lower intensity peaks from azoxybenzene and additional peaks at 6.85–6.93 and 7.14–7.25 ppm from phenylhydroxylamine, suggesting that both "indirect" and "direct" reactions happened; while the addition of 3.4 mM TBA switched the reaction to the "direct pathway" and produced phenylhydroxylamine and aniline. We attribute this switching to the effective quenching of $SO_4^{\bullet-}$ radicals at high concentrations of TBA. This result also demonstrated that $SO_4^{\bullet-}$ is likely the key radical responsible for altering the reaction pathway in the CdS QDs–Na_2SO_3 system. The reaction product, pathway, and related reaction conditions are summarized in Table 1.

Hole scavengers have been reported to change the exciton dynamics and charge carrier transfer from QDs to other species in the catalytic reaction system through optical spectroscopy.[39–42] For example, Gebre *et al.* showed that the addition of triethylamine as a hole scavenger facilitated the electron transfer rate between Cd_3P_2 QDs and *fac*-Re(4,4′-R_2-bpy)$(CO)_3Cl$ (where bpy = bipyridine and R = COOH) (ReC0A).[19] In our work, steady-state and time-resolved photoluminescence (PL) and transient absorption (TA) spectroscopy are used to examine the interaction of Na_2SO_3 with the CdS QDs. The PL spectrum of CdS QDs has two distinct bands that are centered at 475 nm and 650 nm (Fig. 3a). The peak at 475 nm is attributed to the band-edge emission, while the broad red-shifted peak at 650 nm is assigned to trap-state emission arising from the recombination between excited electrons/holes with the holes/electrons trapped by surface defects.[43,44] After the addition of 2 mM Na_2SO_3, the trap-state emission is significantly reduced. Moreover, PL of

Table 1 Reaction pathways under different conditions

Purged gas	Na_2SO_3 (mM)	$SO_4^{\bullet-}$ scavenger TBA (mM)	Reaction time (hr)	Product(s)	Reaction pathway
House N_2	2	0	6	PHA/Aniline	Direct
House N_2	4	0	6	PHA/Aniline	Direct
House N_2	8	0	6	PHA/Aniline	Direct
House N_2	12	0	6	Azoxybenzene	Indirect
House N_2	16	0	6	Azoxybenzene	Indirect
House N_2	24	0	6	Azoxybenzene	Indirect
Air	16	0	4	Azoxybenzene	Indirect
Tank N_2	16	0	4	PHA/Aniline	Direct
Tank Ar	16	0	4	PHA/Aniline (trace)	Direct
House N_2	16	1.7	4	PHA/Azoxybenzene	Mixed
House N_2	16	3.4	4	PHA/Aniline	Direct

PHA represents phenylhydroxylamine.

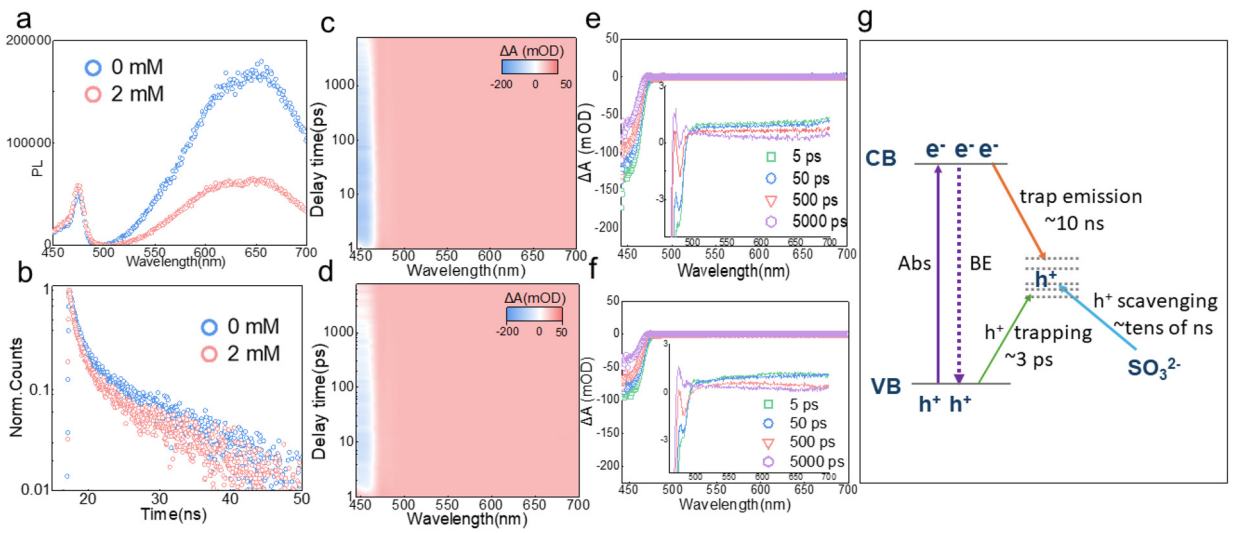

Fig. 3 (a) Photoluminescence spectra of CdS QDs with 0 or 2 mM of Na_2SO_3. (b) PL decays CdS QDs with 0 or 2 mM of Na_2SO_3 measured at 650 nm. Pseudo color TA maps of (c) CdS QDs and (d) CdS QDs with 2 mM Na_2SO_3. ΔA spectra at different time delays of (e) CdS QDs and (f) CdS QDs with 2 mM Na_2SO_3 (inset: magnified ΔA spectra from 460 nm to 700 nm). (g) Schematic illustration of the photophysical processes and timescales.

the QDs with 2 mM Na_2SO_3 measured at 650 nm showed a faster decay (weighted average lifetime 8.2 ns) compared to that of the QDs alone (weighted average lifetime of 10.5 ns), suggesting a dynamic quenching process where SO_3^{2-} ions donate electrons to the CdS QDs (Fig. 3b). Details of the lifetime determination are available in the SI. We do not rule out the possibility for SO_3^{2-} to passivate the QD surface and reduce the number of traps. Increasing the Na_2SO_3 concentration from 4 mM to 24 mM caused slight variations in both the PL intensity and decays at 650 nm, suggesting the quenching effect reaches saturation at 2 mM Na_2SO_3 (Fig. S5a). In contrast, the PL intensity and decays of the band-edge emission peaked at 475 nm only varied slightly between 0 to 24 mM Na_2SO_3, indicating that the quenching process of trap-state emission did not have much influence on the band-edge exciton recombination. The results from TA spectroscopy further support this conclusion, as detailed below.

TA spectroscopic measurements were carried out on CdS QDs mixed with varying concentrations of Na_2SO_3. Fig. 3c–f presents the two-dimensional pseudo-color TA map and ΔA spectra of CdS QDs with 0 and 2 mM Na_2SO_3. A distinct negative signal (~450 nm) from ground-state exciton bleaching was observed in both samples.[45] In addition, a weak broad positive signal appears at 500–700 nm with a rise time of 3–4 ps. This signal is attributed to the photoinduced absorption of the holes trapped to the surface according to previous studies.[46,50] The exciton bleaching kinetics of the QDs at 450 nm with 0–24 mM Na_2SO_3 are similar to each other (Fig. S8a). This result shows that a hole scavenger, Na_2SO_3, does not change the direct exciton recombination,[49,50] consistent with that revealed by the PL decays of the QD samples at 475 nm. The hole absorption decay kinetics at 600 nm were also similar without and with Na_2SO_3 (Fig. S8b). There is a slight variation (up to 5%) in the ΔA values at 5 ps delay time for the band-edge exciton bleach signal at 452 nm and for the hole absorp-

tion signal integrated from 580 to 620 nm when Na_2SO_3 was added (Fig. S9). The addition of hole scavengers did not significantly change the TA signal or kinetics, possibly because of the following reasons. One, the CdS QDs are capped with 3-mercaptopropionic acid. The –COOH groups are deprotonated under the reaction pH of 9–11, leaving the QD surface negatively charged. Therefore, the QDs could have repelled SO_3^{2-} due to electrostatic interactions, making them harder to adsorb onto the QD surface to scavenge the holes. Although the concentration of SO_3^{2-} is much higher than that of the QDs in the solution ($[SO_3^{2-}]:[QD] = 5.7 \times 10^3 - 6.9 \times 10^4 : 1$), the SO_3^{2-} ions on the QD surface will only be a portion. Thus, the number of holes scavenged may be too low to cause a detectable change in the overall TA signal ($\Delta A \sim 2$–3 mOD for the hole absorption band), but still yield enough sulfur-containing radicals to affect the nitrobenzene reduction. Two, it is possible that the $SO_3^{\bullet-}$ radicals stay attached to the QD surface instead of diffusing away after scavenging the holes. The assumption of the adsorption of sulfur-containing radicals (such as $SO_3^{\bullet-}$ and $SO_4^{\bullet-}$) on the QD surface is logical and reasonable, considering their role in dictating the reaction pathway of nitrobenzene reduction. Since photoreduction of nitrobenzene happens on the CdS QD surface, it is necessary for these radicals to stay on the surface to influence the reaction pathway. This assumption is further supported by the Density Functional Theory (DFT) results shown below. Third, the hole absorption signal probed by TA is from the trapped holes on the CdS QD surface as discussed above. The rise of the hole absorption signal indicates that hole trapping is fast, on the time scale of 2–3 ps. On the other hand, when 2 mM SO_3^{2-} was added to the solution, the lifetime of the trap-state emission ($\lambda_{max} \sim 650$ nm, Fig. S5) is reduced from 10.5 ns to 8.2 ns (Table S1). Assuming this reduction is because of SO_3^{2-} scavenging the trapped holes (illustrated in Fig. 3g), we estimated the rate of hole scavenging to be 2.7×10^7 s^{-1}, which means that hole scavenging takes tens of ns (calculation details shown in SI). This time scale is much longer than that probed by TA spectroscopy (sub-ps to ~8 ns); therefore, on top of a likely small number of scavengers on the surface, there was no clear change in the TA signal of the trapped holes within the time of the TA measurements.

To better understand the role of surface-adsorbed $SO_4^{\bullet-}$ in modulating the reaction pathway of nitrobenzene on CdS QDs, we conducted density functional theory (DFT) calculations focusing on the key hydrogenation step from *PhN to *PhNH (see details of these calculations in DFT methods). As shown in Fig. S11, this intermediate transformation serves as a critical branch point between the direct reduction pathway (leading to aniline) and the indirect coupling pathway (leading to azoxybenzene).[24] We first examined the adsorption geometries of *PhN on the CdS(111) surface. Two distinct adsorption modes were identified: a monodentate configuration in which the nitrogen of *PhN binds directly to surface sulfur (Fig. 4a), and a bidentate configuration involving dual interactions (Fig. 4d). The monodentate mode was found to be thermodynamically more stable, with an adsorption energy (ΔE_{ads}) of −2.17 eV, compared to −0.83 eV for the bidentate structure. This suggests that the monodentate configuration is likely the dominant adsorption state under reaction conditions. The reaction energy for the hydrogenation of *PhN to form *PhNH (ΔE_{PhNH}) was next evaluated for the two configurations. In the absence of $*SO_4^{\bullet-}$, hydrogenation of *PhN was found to be favorable for both configurations, but more so for the bidentate mode (Fig. 4d, $\Delta E_{PhNH} = -2.19$ eV) than for the monodentate one (Fig. 4b, $\Delta E_{PhNH} = -1.40$ eV). This indicates that while the monodentate structure dominates the surface population,

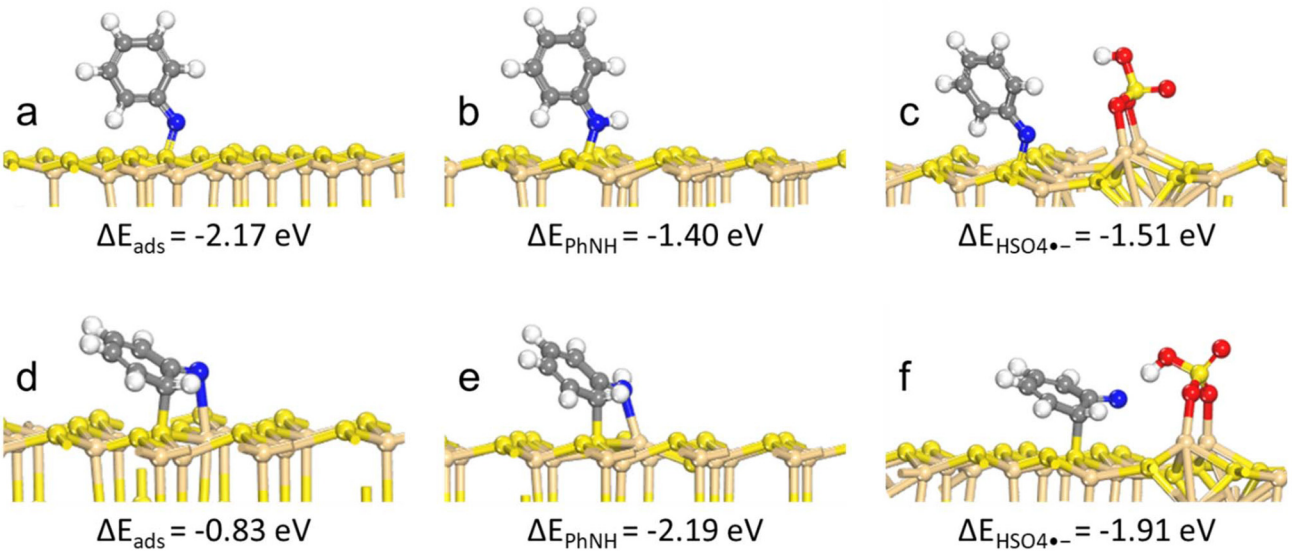

Fig. 4 (a) and (d) Adsorption configurations for *PhN on the CdS(111) surface. (b) and (e) Hydrogenation of *PhN to form *PhNH for the two configurations on the surface. (c) and (f) Hydrogenation of $*SO_4^{\bullet-}$ to form $*HSO_4^{\bullet-}$ for the two configurations on the surface. H, white; C, gray; N, blue; O, red; S, yellow; Cd, gold.

the bidentate species may serve as a more reactive intermediate for reduction.

We then turn to the scenario involving the presence of $^*SO_4^{\bullet-}$. For the monodentate configuration, the reaction energy for the hydrogenation of $^*SO_4^{\bullet-}$ to form $^*HSO_4^{\bullet-}$ ($\Delta E_{HSO_4^-}$) was found to be −1.51 eV, suggesting that $^*SO_4^{\bullet-}$ can effectively abstract hydrogen from *PhNH (Fig. 4c). A similar hydrogenation abstraction could also occur for the bidentate configuration (Fig. 4f). Here, the hydrogen bonding between $^*HSO_4^{\bullet-}$ and *PhN results in an even more favorable $\Delta E_{HSO_4^-}$ of −1.91 eV. Although $\Delta E_{HSO_4^-}$ is not more favorable than ΔE_{PhNH} in the bidentate configuration, statistically a considerable fraction of surface hydrogen can be consumed by $^*SO_4^{\bullet-}$, especially at elevated $^*SO_4^{\bullet-}$ concentrations. These results support a mechanism governed by competitive hydrogenation: in the presence of $^*SO_4^{\bullet-}$, surface hydrogen is preferentially consumed by $^*SO_4^{\bullet-}$ rather than by *PhN intermediate. This competition suppresses direct hydrogenation of *PhN to form *PhNH and instead facilitates an indirect coupling pathway. Such a shift aligns with the experimentally observed change in product distribution at higher Na_2SO_3 concentrations. Overall, the DFT calculations offer theoretical support for $SO_4^{\bullet-}$-mediated modulation of photocatalytic selectivity.

Conclusions

In conclusion, we have shown that the concentration of hole scavenger Na_2SO_3 has a significant impact in the reaction pathways and final products of nitrobenzene reduction using CdS QDs as the catalyst. In particular, we have identified a transition from a direct reduction to indirect coupling when the concentration of Na_2SO_3 increases, even though it is always in excess compared to that of the CdS QDs. ESR spectroscopy and control experiments proved the existence of $SO_4^{\bullet-}$ radicals and revealed its critical impact in changing the reaction pathway. Steady-state and time-resolved PL, alongside fs-TA suggested that SO_3^{2-} scavenged the holes trapped on the CdS surface, turned into $SO_3^{\bullet-}$ and eventually became $SO_4^{\bullet-}$ in the presence of excess SO_3^{2-} and dissolved O_2. DFT calculations provide theoretical support for the role of $SO_4^{\bullet-}$ in modulating photocatalytic selectivity. This study highlights the importance of the quantity of hole scavengers in photocatalytic reactions, where they are typically used in excess without careful consideration of the quantity. Our results indicate that systematically varying the scavenger concentration can influence the formation of radical intermediates during photocatalysis. Such an effect may also occur in other photocatalytic systems with similar hole dynamics and radical formation pathways.

Materials and methods

Chemicals

Sulfur powder (S, 325 mesh, 99.5%), azoxybenzene (AOB, 98%+), and benzyltrimethylammonia hydroxide 40% w/w in methanol (Triton B) were obtained from Alfa Aesar. Methanol-d_4 (CD_3OD, 99.8%) and deuterium dioxide (D_2O, 99.9%) were purchased from Cambridge Isotope Laboratory. 2-Amino-2-hydroxymethyl-propane-1,3-diol (tris buffer, R99.8%) was purchased from Thermo Fisher Scientific. 3-Mercaptopropionic acid (3-MPA, 99%+) was purchased from Acros Organics. Nitrobenzene (NB, R99.0%), cadmium oxide (CdO, R99.99%), oleic acid (OA, 90%), diethyl ether (99.0%), sodium sulfite (Na_2SO_3, 98%), ethyl acetate (99.7%), 1-octadecene (ODE, 99%), *N*-phenylhydroxylamine (PHA, R95.0%), aniline (R99.5%), acetone (HPLC, R99.9%), and ethanol (99.8%) were purchased from Sigma-Aldrich. 5,5-Dimethyl-1-pyrroline *N*-oxide (DMPO) was purchased from Dojindo. Nitrogen (N_2) and argon (Ar) gases were purchased from Airgas, each with a purity of 99.999%. All chemicals were used without further purification.

Photocatalytic experiments

CdS QDs were prepared using a slightly modified procedure from the previous work and the details are included in the SI.[18] A total of 3 mL solution was prepared for each sample, consisting of 0.2 M (72.6 mg) tris buffer, 0/2/4/8/12/16/24 mM sodium sulfite, 2.5 mM nitrobenzene, and 0.35 μM CdS QDs in D_2O : CD_3OD (v : v = 4 : 1) solvent mixture to form a homogenous light-yellow solution. The solution was then transferred into a quartz cuvette, sealed with septa. Then, each solution was purged with protective gas (house N_2, and N_2 or Ar from Airgas) for 5 minutes. Photocatalytic reduction reactions were carried out using a blue LED (ABI, 12 W, PAR38, 450–460 nm) for illumination over specified reaction times. Finally, a 0.6 mL sample was taken from each reaction solution without further purification and measured with NMR.

Spectroscopic instruments and characterization

Absorption spectra of the QDs were collected by an Agilent Technologies Cary-60 UV–vis spectrometer. Transmission electron microscopy (TEM) images were taken using a TechnaiT-12 microscope. ^{1}H NMR spectra for all samples were acquired using a Bruker Avance III 300 MHz NMR spectrometer. Fluorescence was tested by a Horiba FluoroMax Plus fluorometer. PL decay was measured using the Mini-tau model of Edinburgh Instruments with a 405 nm pulsed laser, and the emission was collected between 425–475 nm and 625–675 nm. X-ray diffraction (XRD) patterns of the CdS QDs were recorded on a Bruker D2 diffractometer with Bragg–Brentano θ–2θ geometry (30 kV and 10 mA) by using a nickel filter with a Cu Kα radiation source.

ESR experiments

The electron spin resonance (ESR) measurements were performed at room temperature utilizing a Bruker EMXnano spectrometer equipped with an X-band frequency. The parameters for ESR tests are as follows: 9.62–9.64 GHz microwave frequency, 0.6310 mW microwave power, 9.27 s sweep time, 0.6 Gauss modulation amplitude, and 100 kHz modulation frequency. For ESR measurements, a total sample volume of

20 μL was prepared, with DMPO (1.12 M), CdS QDs (0.35 μM), and 2 mM or 16 mM Na_2SO_3, with ultrapure water as the solvent. The sample solutions were injected into a 0.8 mm glass capillary using a volumetric syringe, and the capillary was then placed into a 5 mm gastight Suprasil ESR tube from Wilmad LabGlass. Some of the samples were degassed for 5 minutes with N_2 prior to measurements. During ESR measurements, samples were illuminated using a 100 W mercury arc lamp equipped with a mechanical shutter and a 455 nm long-pass filter, which was connected *via* a fiber optic to the spectrometer. Spin adducts were identified by comparison of hyperfine splitting values to literature.[33] Hyperfine splitting values were extracted from experimental spectra by least squares fit using the EasySpin program for Matlab.[51] Details of the fitting and simulation process are described in the SI.

Femtosecond transient absorption (TA) measurements

For femtosecond TA (fsTA) measurements, 0.6 mL of solution containing 0.35 μM CdS QDs and 0/2/4/8/12/16/24 mM of Na_2SO_3 were prepared in D_2O solvent. The samples were transferred to quartz cells with a path length of 2 mm. The fsTA setup was based on Helios Fire (Ultrafast Systems) coupled to a femtosecond laser system (Coherent). The system consists of an AStrella one-box Ti: sapphire amplifier. The pulse width was 35 fs full width at half maximum at 800 nm with an energy of 5.0 mJ per pulse at a 1 kHz repetition rate. The output of the amplifier was divided by beam splitters. One beam (48% of the total power) was used as the input for an OPerA Solo optical parametric amplifier (Coherent), which provided a pump pulse in the UV-visible (UV-vis) region. The energy of the pump beam was adjusted to 0.5–1.0 μJ by a neutral density filter. Another beam (2% of the total power) was used to generate white light continuum probe pulses in the Helios spectrometer. Samples were scanned at 400 delay time points, and the integration time was set to 0.2 s. During the measurements, samples were pseudo-randomly translated to avoid photodegradation by using a translating sample holder (Ultrafast Systems). A 1024-pixel CMOS sensor was used for detection. The raw data were processed by background subtraction and chirp correction using the Surface Xplore software (Ultrafast Systems).

DFT calculations

Spin-polarized DFT calculations were performed using the Vienna *ab initio* simulation package (VASP).[47,48] The electron exchange–correlation was represented by the functional of Perdew, Burke, and Ernzerhof (PBE) of generalized gradient approximation (GGA).[49] The ion-electron interaction was described using the projector-augmented wave (PAW) method.[50] The plane-wave cutoff was set to 400 eV, and a conjugate gradient method was applied to relax the geometry until the interatomic forces were less than 0.025 eV $Å^{-1}$. The Brillouin zone was sampled using a 3 × 3 × 1 Monkhorst–Pack *k*-point mesh. The experimental lattice parameter from XRD measurement (Fig. S10) of 5.91 Å was used for CdS, and the CdS(111) surface was modeled using a 4 × 4 supercell with three atomic layers. The top two atomic layers, including adsorbates, were allowed to relax, while the bottom one atomic layer was fixed during optimization. Vacuum space in the *z* direction was set to be 20 Å to avoid unphysical interactions.

The adsorption energy of *PhN was calculated using the equation $\Delta E = E_{slab+PhN} - E_{slab} - E_{PhN}$, where $E_{slab+PhN}$, E_{slab}, and E_{PhN} represent the energies of the CdS slab with adsorbed PhN, the clean CdS slab, and the isolated PhN intermediate, respectively. The reaction energy for the hydrogenation of *PhN was determined using $\Delta E = E_{slab+PhNH} - E_{slab+PhN} - 1/2E_{H_2}$, where $E_{slab+PhNH}$ and $E_{slab+PhN}$ are the energies of the CdS slab with adsorbed PhNH and PhN, respectively. Similarly, the reaction energy for the hydrogenation of $*SO_4^{\bullet-}$ was calculated using $\Delta E = E_{slab+HSO_4^-} - E_{slab+SO_4^-} - 1/2E_{H_2}$, where $E_{slab+HSO_4^-}$ and $E_{slab+SO_4^-}$ correspond to the energies of the CdS slab with adsorbed $HSO_4^{\bullet-}$ and $SO_4^{\bullet-}$, respectively.

We note that the present DFT calculations are simplified and do not capture the full complexity of the experimental system. First, the CdS(111) surface was considered in the models because our XRD data showed that the (111) facet was the dominant exposed surface. Nevertheless, other surface facets may also be present in the experimentally obtained CdS QDs and could influence adsorption configurations and reaction energetics. Second, although we analyzed the adsorption configurations of *PhN in detail, we did not perform a systematic analysis of the adsorption geometries of $*SO_4^{\bullet-}$ radicals, which may affect the accuracy of the predicted competitive hydrogenation mechanism. Third, the CdS QDs used in experiments are capped with 3-mercaptopropionic acid (3-MPA), which could modify surface energetics and adsorption behaviors. These ligands were not included in the current calculations for computational simplicity. Future work incorporating multiple surface facets, $*SO_4^{\bullet-}$ adsorption configurations, and explicit ligand effects will provide a more comprehensive understanding of the photocatalytic mechanism.

Author contributions

The manuscript was written through contributions of all authors. All authors have given approval to the final version of the manuscript.

Conflicts of interest

The authors declare no competing financial interest.

Data availability

All data generated in this study, including the raw data from DFT calculations and experiments as well as the data required to reproduce the results, will be shared. The data will be deposited in the open-access repository Figshare and made publicly available immediately after the publication of this work.

Supplementary information: experimental details, additional NMR spectra, UV-vis absorption, TEM, ESR, steady-state and time-resolved PL, TA, and XRD (PDF). See DOI: https://doi.org/10.1039/d5nr03085d.

Acknowledgements

This work was partially supported by the donors of ACS Petroleum Research Fund under Doctoral New Investigator Grant 67453-DNI6. G. H. served as Principal Investigator on ACS PRF 67453-DNI6 that provided support for C. B. This research used resources of the National Energy Research Scientific Computing Center, a DOE Office of Science User Facility supported by the Office of Science of the U.S. Department of Energy under Contract No. DE-AC02-05CH11231 using NERSC award BES-ERCAP0031261.

References

1 V. Alevato, D. Streater, J. Huang and S. Brock, Effect of Crystal Structure on the Aggregation of CdS Quantum Dots: Consequences for Photophysical Properties and Photocatalytic Hydrogen Evolution Activity, *J. Phys. Chem. C*, 2024, **128**(27), 11239–11246.

2 Y. Yu, A. Kipkorir, M. Y. Choi and P. V. Kamat, Photocatalytic Membrane for Hydrogen Evolution: Directed Electron and Hole Transfer across Pt–$AgInS_2$–Nafion, *ACS Mater. Lett.*, 2024, **6**(5), 1856–1862.

3 H. B. Yang, J. W. Miao, S. F. Hung, F. W. Huo, H. M. Chen and B. Liu, Stable Quantum Dot Photoelectrolysis Cell for Unassisted Visible Light Solar Water Splitting, *ACS Nano*, 2014, **8**(10), 10403–10413.

4 T. F. Yeh, C. Y. Teng, S. J. Chen and H. Teng, Nitrogen-doped graphene oxide quantum dots as photocatalysts for overall water-splitting under visible light illumination, *Adv. Mater.*, 2014, **26**(20), 3297–3303.

5 Y. He, P. Y. Hu, J. J. Zhang, G. J. Liang, J. G. Yu and F. Y. Xu, Boosting Artificial Photosynthesis: CO_2 Chemisorption and S-Scheme Charge Separation via Anchoring Inorganic QDs on COFs, *ACS Catal.*, 2024, **14**(3), 1951–1961.

6 M. Chhetri and P. V. Kamat, Vectorial Charge Transfer across Bipolar Membrane Loaded with CdS and Au Nanoparticles, *J. Phys. Chem. C*, 2021, **125**(12), 6870–6876.

7 S. Lian, M. S. Kodaimati and E. A. Weiss, Photocatalytically Active Superstructures of Quantum Dots and Iron Porphyrins for Reduction of CO_2 to CO in Water, *ACS Nano*, 2018, **12**(1), 568–575.

8 F. Arcudi, L. Dordevic, B. Nagasing, S. I. Stupp and E. A. Weiss, Quantum Dot-Sensitized Photoreduction of CO2 in Water with Turnover Number > 80,000, *J. Am. Chem. Soc.*, 2021, **143**(43), 18131–18138.

9 Y. F. Xu, M. Z. Yang, B. X. Chen, X. D. Wang, H. Y. Chen, D. B. Kuang and C. Y. Su, A $CsPbBr_3$ Perovskite Quantum Dot/Graphene Oxide Composite for Photocatalytic CO_2 Reduction, *J. Am. Chem. Soc.*, 2017, **139**(16), 5660–5663.

10 H. Park, H. H. Ou, A. J. Colussi and M. R. Hoffmann, Artificial photosynthesis of C1-C3 hydrocarbons from water and CO_2 on titanate nanotubes decorated with nano-particle elemental copper and CdS quantum dots, *J. Phys. Chem. A*, 2015, **119**(19), 4658–4666.

11 D. G. Xie, C. X. Tang, D. Li, J. R. Yuan and F. G. Xu, Enhanced Photo-Fenton Catalytic Performance toward Acid Orange II by FeOCl/CdS Quantum Dot Composites: Density Functional Theory Calculations and Mechanistic Insights, *J. Phys. Chem. C*, 2024, **128**(8), 3295–3306.

12 A. A. P. Mansur, H. S. Mansur, F. P. Ramanery, L. C. Oliveira and P. P. Souza, "Green" colloidal ZnS quantum dots/chitosan nano-photocatalysts for advanced oxidation processes: Study of the photodegradation of organic dye pollutants, *Appl. Catal., B*, 2014, **158–159**(1), 269–279.

13 L. X. Zhang, M. Y. Qi, Z. R. Tang and Y. J. Xu, Heterostructure-Engineered Semiconductor Quantum Dots toward Photocatalyzed-Redox Cooperative Coupling Reaction, *Research*, 2023, **6**(0073), 1–11.

14 I. N. Chakraborty, P. Roy and P. P. Pillai, Visible Light-Mediated Quantum Dot Photocatalysis Enables Olefination Reactions at Room Temperature, *ACS Catal.*, 2023, **13**(11), 7331–7338.

15 J. Schneider and D. W. Bahnemann, Undesired Role of Sacrificial Reagents in Photocatalysis, *J. Phys. Chem. Lett.*, 2013, **4**(20), 3479–3483.

16 M. Y. Qi, X. N. Shao, Z. R. Tang and Y. J. Xu, Light-Controlled Switch for Divergent Coupling of Thiols to Disulfides/Thioethers over CdS Quantum Dots, *ACS Mater. Lett.*, 2025, **7**(4), 1533–1539.

17 N. Jin, Y. Sun, W. Shi, P. Wang, Y. Nagaoka, T. Cai, R. Wu, L. Dube, H. N. Nyiera, Y. Liu, T. Mani, X. Z. Wang, J. Zhao and O. Chen, Type-I CdS/ZnS Core/Shell Quantum Dot-Gold Heterostructural Nanocrystals for Enhanced Photocatalytic Hydrogen Generation, *J. Am. Chem. Soc.*, 2023, **145**(40), 21886–21896.

18 Y. Li, S. Yu, J. L. Xiang, F. Y. Zhang, A. Q. Jiang, Y. G. Duan, C. Tang, Y. H. Cao, H. Guo and Y. Zhou, Revealing the Importance of Hole Transfer: Boosting Photocatalytic Hydrogen Evolution by Delicate Modulation of Photogenerated Holes, *ACS Catal.*, 2023, **13**(12), 8281–8292.

19 S. T. Gebre, L. M. Kiefer, F. H. Guo, K. R. Yang, C. Miller, Y. W. Liu, C. P. Kubiak, V. S. Batista and T. Q. Lian, Amine Hole Scavengers Facilitate Both Electron and Hole Transfer in a Nanocrystal/Molecular Hybrid Photocatalyst, *J. Am. Chem. Soc.*, 2023, **145**(5), 3238–3247.

20 A. W. Mureithi, Y. Sun, T. Mani, A. R. Howell and J. Zhao, Impact of hole scavengers on photocatalytic reduction of nitrobenzene using cadmium sulfide quantum dots, *Cell Rep. Phys. Sci.*, 2022, **3**(5), 1–14.

21 E. A. Gelder, S. D. Jackson and C. M. Lok, The hydrogenation of nitrobenzene to aniline: a new mechanism, *Chem. Commun.*, 2005, **4**(1), 522–524.

22 H. H. Wang, W. Zhang, Y. Q. Liu, M. Pu and M. Lei, First-Principles Study on the Mechanism of Nitrobenzene Reduction to Aniline Catalyzed by a N-Doped Carbon-Supported Cobalt Single-Atom Catalyst, *J. Phys. Chem. C*, 2021, **125**(35), 19171–19182.

23 P. Brezová, P. Tarábek, D. Dvoranová, A. Staško and B. Stanislav, EPR study of photoinduced reduction of nitroso compounds in titanium dioxide suspensions, *J. Photochem. Photobiol., A*, 2003, **155**(1–3), 179–198.

24 Z. J. Li, X. W. Lu, C. Guo, S. Q. Ji, H. X. Liu, C. M. Guo, X. Lu, C. Wang, W. S. Yan, B. Y. Liu, W. Wu, J. H. Horton, S. X. Xin and Y. Wang, Solvent-free selective hydrogenation of nitroaromatics to azoxy compounds over Co single atoms decorated on Nb_2O_5 nanomeshes, *Nat. Commun.*, 2024, **3195**, 15.

25 W. W. Yu, L. H. Qu, W. Z. Guo and X. Z. Peng, Experimental Determination of the Extinction Coefficient of CdTe, CdSe, and CdS Nanocrystals, *Chem. Mater.*, 2003, **15**(14), 2854–2860.

26 W. Deng, H. L. Zhao, F. P. Pan, X. H. Feng, B. Jung, A. Abdel-Wahab, B. Batchelor and Y. Li, Visible-Light-Driven Photocatalytic Degradation of Organic Water Pollutants Promoted by Sulfite Addition, *Environ. Sci. Technol.*, 2017, **51**(22), 13372–13379.

27 X. Gao, P. F. Wang, H. N. Che, W. Liu and Y. H. Ao, Breaking interfacial charge transfer barrier by sulfite for efficient pollutants degradation: a case of $BiVO_4$, *npj Clean Water*, 2023, **6**(42), 1–8.

28 K. Ranguelova and R. P. Mason, New insights into the detection of sulfur trioxide anion radical by spin trapping: radical trapping versus nucleophilic addition, *Free Radical Biol. Med.*, 2009, **47**(2), 128–134.

29 R. E. Huie and C. L. Clifton, Rate constants for hydrogen abstraction reactions of the sulfate radical, SO_4^-. Alkanes and ethers, *Int. J. Chem. Kinet.*, 1989, **21**(8), 611–619.

30 C. L. Clifton and R. E. Huie, Rate constants for hydrogen abstraction reactions of the sulfate radical, SO_4^-, Alcohols, *Int. J. Chem. Kinet.*, 1989, **21**(8), 677–687.

31 P. Piccinini, C. Minero, M. Vincenti and E. Pelizzetti, Photocatalytic interconversion of nitrogen-containing benzenederivative, *J. Chem. Soc.*, 1997, **93**(10), 1993–2000.

32 L. L. Wang, Q. C. Li, Y. Fu, Z. H. Wang, H. Y. Zhu and M. Sillanpää, Undiscovered Spin Trapping Artifacts in Persulfate Oxidation Processes: Implications for Identification of Hydroxyl or Sulfate Radicals in Water, *ACS ES&T Water*, 2023, **3**(2), 532–541.

33 P. L. Zamora and F. A. Villamena, Theoretical and experimental studies of the spin trapping of inorganic radicals by 5,5-dimethyl-1-pyrroline N-oxide (DMPO). 3. Sulfur dioxide, sulfite, and sulfate radical anions, *J. Phys. Chem. A*, 2012, **116**(26), 7210–7218.

34 R. J. Zhao, L. Li, Q. B. Wu, W. Luo, Q. Zhang and C. H. Cui, Spontaneous formation of reactive redox radical species at the interface of gas diffusion electrode, *Nat. Commun.*, 2024, **15**, 8367.

35 Z. S. Wei, F. A. Villamena and L. K. Weavers, Kinetics and mechanism of ultrasonic activation of persulfate: an in situ EPR spin trapping study, *Environ. Sci. Technol.*, 2017, **51**(6), 3410–3417.

36 Y. Wu, D. Y. Xing, L. N. Zhang, H. L. Suo and X. D. Zhao, Application of a novel heterogeneous sulfite activation with copper(I) sulfide (Cu_2S) for efficient iohexol abatement, *RSC Adv.*, 2022, **12**(13), 8009–8018.

37 Z. Wang, J. Jiang, S. Y. Pang, Y. Zhou, C. T. Guan, Y. Gao, J. Li, Y. Yang, W. Qiu and C. C. Jiang, Is Sulfate Radical Really Generated from Peroxydisulfate Activated by Iron(II) for Environmental Decontamination, *Environ. Sci. Technol.*, 2018, **52**(19), 11276–11284.

38 I. N. Chakraborty, V. Jain, P. Roy, P. Kumar, C. P. Vinod and P. P. Pillai, Photocatalytic Regeneration of Reactive Cofactors with InP Quantum Dots for the Continuous Chemical Synthesis, *ACS Catal.*, 2024, **14**(9), 6740–6748.

39 Y. Ye, X. L. Wang, S. Ye, Y. X. Xu, Z. C. Feng and C. Li, Charge-Transfer Dynamics Promoted by Hole Trap States in CdSe Quantum Dots–Ni^{2+} Photocatalytic System, *J. Phys. Chem. C*, 2017, **121**(32), 17112–17120.

40 M. C. Sekhar, K. Santhosh, J. P. Kumar, N. Mondal, S. Soumya and A. Samanta, CdTe Quantum Dots in Ionic Liquid: Stability and Hole Scavenging in the Presence of a Sulfide Salt, *J. Phys. Chem. C*, 2014, **118**(32), 18481–18487.

41 J. R. Lee, W. Li, A. J. Cowan and F. Jäckel, Hydrophilic, Hole-Delocalizing Ligand Shell to Promote Charge Transfer from Colloidal CdSe Quantum Dots in Water, *J. Phys. Chem. C*, 2017, **121**(28), 15160–15168.

42 K. F. Wu, H. M. Zhu, Z. Liu, W. Rodriguez-Cordoba and T. Q. Lian, Ultrafast charge separation and long-lived charge separated state in photocatalytic CdS-Pt nanorod heterostructures, *J. Am. Chem. Soc.*, 2012, **134**(25), 10337–10340.

43 K. R. Gopidas, M. Bohorquez and P. V. Kamat, Photophysical and photochemical aspects of coupled semiconductors: charge-transfer processes in colloidal cadmium sulfide-titania and cadmium sulfide-silver(I) iodide systems, *J. Phys. Chem.*, 1990, **94**(16), 6435–6440.

44 K. F. Wu, Y. L. Du, H. Tang, Z. Y. Chen and T. Q. Lian, Efficient Extraction of Trapped Holes from Colloidal CdS Nanorods, *J. Am. Chem. Soc.*, 2015, **137**(32), 10224–10230.

45 J. Huang, Z. Q. Huang, S. Y. Jin and T. Q. Lian, Exciton Dissociation in CdSe Quantum Dots by Hole Transfer to Phenothiazine, *J. Phys. Chem. C*, 2008, **112**(1), 19734–19738.

46 S. Das, S. Rakshit and A. Datta, Interplay of Multiexciton Relaxation and Carrier Trapping in Photoluminescent CdS Quantum Dots Prepared in Aqueous Medium, *J. Phys. Chem. C*, 2020, **124**(51), 28313–28322.

47 K. F. Wu, Z. Liu, H. M. Zhu and T. Q. Lian, Exciton annihilation and dissociation dynamics in group II–V Cd_3P_2 quantum dots, *J. Phys. Chem. A*, 2013, **117**(29), 6362–6372.

48 D. Jasrasaria, J. P. Philbin, C. Yan, D. Weinberg, A. P. Alivisatos and E. Rabani, Sub-bandgap photoinduced transient absorption features in CdSe nanostructures: The role of trapped holes, *J. Phys. Chem. C*, 2020, **124**(31), 17372–17378.

49 K. J. Schnitzenbaumer, T. Labrador and G. Dukovic, Impact of chalcogenide ligands on excited state dynamics in CdSe quantum dots, *J. Phys. Chem. C*, 2015, **119**(23), 13314–13324.
50 G. Grimaldi, J. J. Geuchies, W. Van Der Stam, I. Du Fossé, B. Brynjarsson, N. Kirkwood, S. Kinge, L. D. Siebbeles and A. J. Houtepen, Spectroscopic evidence for the contribution of holes to the bleach of Cd-chalcogenide quantum dots, *Nano Lett.*, 2019, **19**(5), 3002–3010.
51 S. Stefan and A. Schweiger, EasySpin, a comprehensive software package for spectral simulation and analysis in EPR, *J. Magn. Reson.*, 2006, **178**(1), 42–55.